mater.scichina.com link.springer.com

Published online 29 May 2020 | https://doi.org/10.1007/s40843-020-1312-7
Sci China Mater 2020, 63(9): 1663–1671

Facile one-step vulcanization of copper foil towards stable Li metal anode

Danqi He[1], Yaqi Liao[1], Zexiao Cheng[1], Xiahan Sang[2], Lixia Yuan[1], Zhen Li[1*] and Yunhui Huang[1*]

ABSTRACT **Lithium metal has been regarded as the ultimate anode for next-generation rechargeable batteries with high energy density. However, its high reactivity and dendrite growth seriously limit its commercial application, which can be well addressed by realizing uniform Li deposition. Here, we report a facile and scalable one-step vulcanization method to modify commercial Cu foil with lithophilic Cu_2S. The *in situ* formed Cu_2S layer can not only promote the homogeneous deposition of Li *via* its lithophilic nature, but also benefit the formation of a stable solid-electrolyte interphase during initial activation. The Cu_2S-modified Cu current collector realizes dendrite-free Li plating/stripping and thus exhibits stable cycling performance with a high Coulombic efficiency, even with a large capacity of 4 mA h cm^{-2}. A full-cell consisting of a Cu_2S/Cu-Li anode and a $LiFePO_4$ cathode exhibits greatly improved cycling stability and enhanced Coulombic efficiency, demonstrating the effectiveness and practicability of the proposed Cu_2S/Cu foil in the field of rechargeable Li metal batteries.**

Keywords: lithium metal anode, current collector, lithophilic layer, copper sulfide, electrochemical performance

INTRODUCTION

Lithium-ion batteries (LIBs) have completely changed our lifestyle in recent decades. With the emergence of many new applications, current commercial LIBs can hardly meet the increasing demands of high energy density [1–5]. Lithium metal has been considered as one of the most promising anodes for next-generation batteries, due to its quite high theoretical specific capacity (3860 mA h g^{-1}) and extremely low redox potential (−3.04 V *vs.* standard hydrogen electrode) [6–8]. However, the Li dendrite growth issue is a main challenge for Li metal anodes [9–11]. The deposition of Li^+ on the interface is usually faster than its diffusion, so the growth of Li tends to be dendritic form, which may puncture the separator, induce short circuits, and even cause severe thermal runaway. The relatively high Fermi energy and large exposed surface area of a Li dendrite also lead to serious reactions with the liquid electrolyte. The formation of unstable solid electrolyte interphase (SEI) on the anode surface and the continuous consumption of electrolyte may cause low Coulombic efficiency and poor cycle stability of the full-cells [12–14]. Accordingly, this series of problems generated by Li dendrite growth greatly limit the commercial application of Li metal anodes. In recent years, extensive efforts have been devoted to resolving or mitigating the Li dendrite issue: (1) constructing uniform and compact SEI by *in situ* and *ex situ* methods is an efficient way. For example, introducing various additives ($LiNO_3$, Li_2S_6, HF, $Cu(CH_3COO)_2$, LiF) or optimizing the solvents to react with Li metal can *in situ* form a stable SEI layer [15–17]. It is also practicable to *ex situ* fabricate artificial SEI layers, including organic, inorganic, and hybrid films [18–21]. Although some SEI could effectively protect the Li metal anode during the Li^+ plating and stripping processes, the mechanical ability of thin SEI films is not steady enough to endure high areal capacity and prolonged cycles. (2) Using solid state electrolytes, such as solid polymer electrolytes or ceramic electrolytes, can physically prevent the growth of Li dendrites [22,23]. However, the ionic conductivity of the solid electrolyte is still not comparable to that of the liquid electrolyte at room temperature, and the non-intimate contact between the solid electrolyte and the Li metal may result in large interfacial impedance. (3) Reducing local deposition current density through employing three-dimensional (3D) current collectors can successfully avoid Li dendrite growth [24–27]. The 3D current collectors have a large

[1] State Key Laboratory of Material Processing and Die and Mold Technology, School of Materials Science and Engineering, Huazhong University of Science and Technology, Wuhan 430074, China
[2] State Key Laboratory of Advanced Technology for Materials Synthesis and Processing, Wuhan University of Technology, Wuhan 430070, China
* Corresponding authors (emails: li_zhen@hust.edu.cn (Li Z); huangyh@hust.edu.cn (Huang Y))

specific surface area to reduce local current density and hence improve the uniformity of Li-ion deposition. However, at the same time, such current collectors (with large surface area) may promote side reactions between the electrolyte and the Li metal, reducing the volumetric energy density of the electrode.

Copper (Cu) foil is the most common anodic current collector. Modifying Cu foil can improve the stability of a Li metal anode [28,29]. One effective strategy is to optimize the surface structure of Cu foil. Guo's group [30] took advantage of a 3D structure and constructed a submicron skeleton on the surface of a Cu current collector to ameliorate the electrochemical deposition behavior of Li^+ ions. Other strategies include reducing the nucleation overpotential and inducing the uniform deposition of Li^+ through various modified layers on Cu foil, such as hexagonal boron nitride, polyacrylonitrile (including polyacrylonitrile with polar functional groups), reduced graphene oxide, ZnO, Si, and Sn [13,31,32]. These modified layers are usually synthesized by complicated methods, such as atomic layer deposition or chemical vapor deposition [28], which may not be easily scaled up for mass production. Thus, it is of great importance to explore and develop new routes for facile and low-cost fabrication of current collectors with lithiophilic surfaces.

Here, we develop a one-step method by simple vulcanization of Cu foil to *in situ* form a modified layer of Cu_2S (Fig. 1a). With the assistance of the Cu_2S lithophilic layer, the nucleation overpotential of Li is significantly lowered and, hence, the deposition of Li^+ ions becomes much more uniform and dense (Fig. 1c). As a result, the prepared Cu_2S/Cu current collector promises stable cycling performance with a high Coulombic efficiency in Li metal cells. A full-cell with Li/Cu_2S/Cu anode and $LiFePO_4$ cathode exhibits good cycling stability and enhanced Coulombic efficiency, demonstrating the effectiveness and practicability of the Cu_2S/Cu foil for rechargeable Li metal batteries.

EXPERIMENTAL SECTION

The Cu_2S/Cu current collector was fabricated by a one-step method. Specifically, commercial Cu foil and pure sulfur powder were sealed within a tube furnace, where the sulfur was located near the Cu foil in the direction of the gas, and then heated to 400°C for 10 min under Ar atmosphere. The Cu_2S/Cu current collector was obtained after the temperature dropped back to room temperature.

The phase constituents were determined by X-ray diffraction (XRD, Bruker D8-Advance) using Cu Kα radiation. The morphologies of all electrodes were observed by field emission scanning electron microscopy (FESEM, FEI Quanta 650 FEG). The high angle annular dark-field (HAADF) images, atomic resolution HAADF images, elemental mappings, and electron energy loss spectroscopy (EELS) were carried out by a double spherical aberration corrected transmission electron microscope (TEM, Thermo Fisher Titan Themis G2 60-300), for

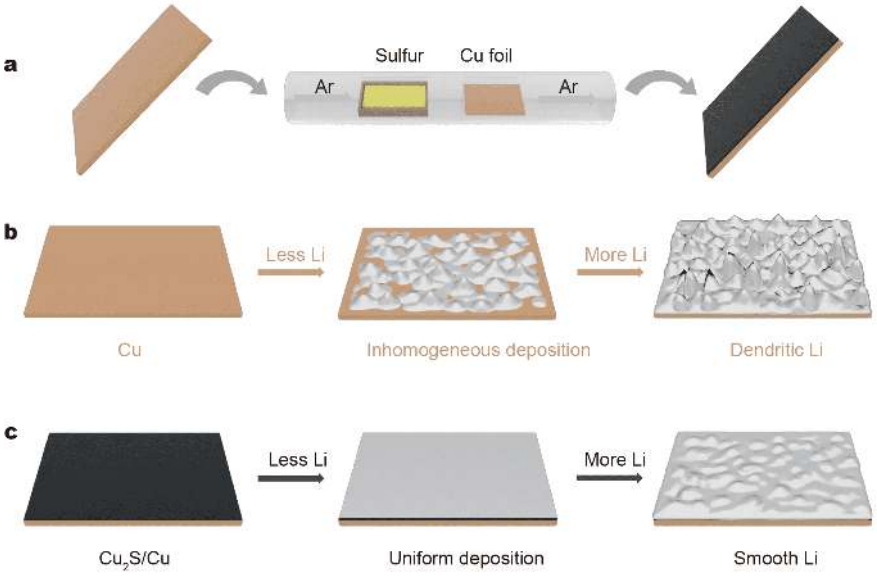

Figure 1 (a) Illustration of the *in situ* fabrication process of the Cu_2S/Cu current collector. Schematics of different Li plating behaviors on (b) Cu and (c) Cu_2S/Cu current collectors.

which the sample was prepared by focused ion beam. To further analyze the SEI layer, X-ray photoelectron spectroscopy (XPS) of S 2p was recorded using a Thermo VG Multilab 2000 spectrometer.

All electrochemical properties were measured with standard CR2032 coin-type cells, all of which were assembled in the argon-filled glove box under the conditions of the oxygen with the water contents both below 0.5 ppm. The electrolyte was 1 mol L^{-1} LiTFSI in a mixture of 1,3-dioxolane (DOL) and dimethoxymethane (DME) (v/v = 1:1) with 2 wt% of $LiNO_3$. CR2032 coin cells were assembled with the Cu_2S/Cu foil or bare Cu foil (both current collectors with 12 mm diameters) as the working electrode, the ether electrolyte, Celgard 2400 as the separator, and Li foil (with the same diameter of 12 mm) as the counter-electrode. The cycling performance was measured on a Land Battery Measurement System (Land, China). To test the Coulombic efficiency, the cells were first cycled in the range of 0–1 V at 0.05 mA for three cycles for the formation of SEI. Then, different Li contents (1 and 4 mA h cm^{-2}) were deposited onto the working electrodes at a current density of 1 mA cm^{-2} and stripped away until the voltage reached 1 V. Electrochemical impedance spectroscopy (EIS) was measured in the stripping state of cells after 50 cycles at a current density of 1 mA cm^{-2} with a capacity of 1 mA h cm^{-2}. The voltage amplitude applied to the coin cells was 5 mV, with the frequency ranging from 100 kHz to 1 Hz. For the symmetric cell test, bare Cu foil or Cu_2S/Cu foil was firstly deposited with 4 mA h cm^{-2} of Li in a half-cell, then taken out for assembling symmetric cells. The cycling performance of the symmetric cell was measured at a current density of 1 mA cm^{-2} with a capacity of 1 or 4 mA h cm^{-2}. For the full-cell test, the cathode electrode was made by mixing 80 wt% of $LiFePO_4$ powder, 10 wt% of Super P, and 10 wt% of polyvinylidene fluoride (PVDF) to form a homogeneous slurry. The slurry was spread onto Al foil and dried in vacuum at 120°C for 24 h. The mass loading of $LiFePO_4$ in the electrode was about 3 mg cm^{-2}. To avoid any additional influence from the usage of the electrolyte, all cells for testing contained 50 μL electrolyte.

RESULTS AND DISCUSSION

Lithophilic experiments of both Cu foil and Cu_2S/Cu foil were simultaneously carried out (Fig. 2a). The yellow Cu foil and black-blue Cu_2S/Cu foil (with the same diameter of 19 mm) were placed in the stain steel cases, and pieces of Li foil (with diameter of 15 mm) were placed onto the Cu foil and Cu_2S/Cu foil, respectively. When heating to 300°C, the sheet-shaped Li foil was quickly melted and turned into a sphere, due to the non-lithophilic ability of

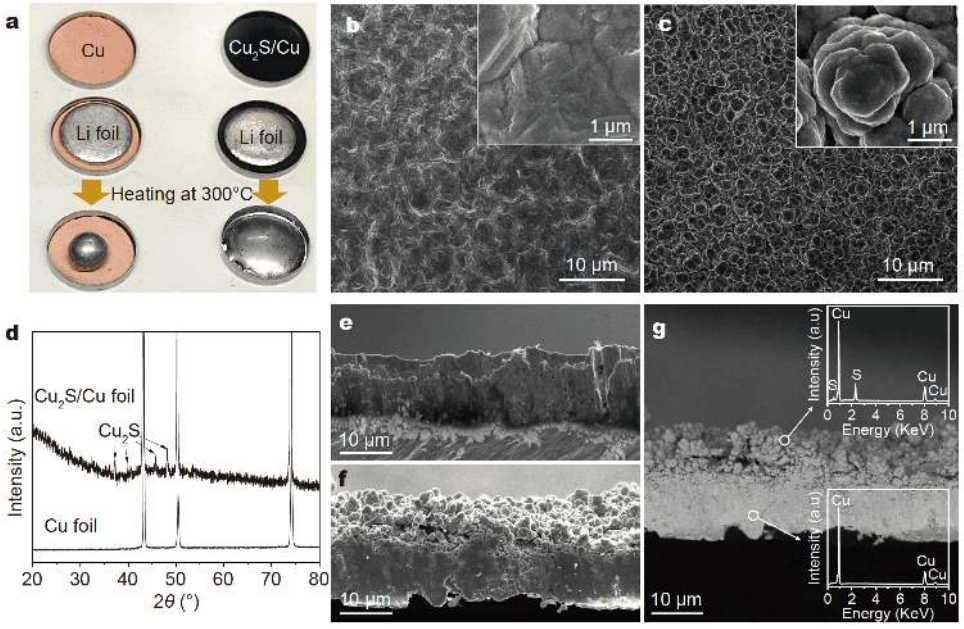

Figure 2 (a) The lithophilic experiment, revealing the lithophilic abilities of both the Cu foil and Cu_2S/Cu foil. The surface morphologies of (b) Cu foil and (c) Cu_2S/Cu foil (the insets are the corresponding enlarged pictures). (d) XRD patterns of both Cu foil and Cu_2S/Cu foil. The cross-sectional images of (e) Cu foil and (f) Cu_2S/Cu foil. (g) The corresponding backscattering electron image of (f) (the insets are energy disperse spectroscopy patterns).

Cu. By contrast, the Li foil on Cu_2S/Cu melted and spread out over the surface of the Cu_2S/Cu foil under the same condition, indicating that Cu_2S has good lithophilic ability.

After vulcanization, the rough surface of the Cu foil (Fig. 2b) is covered by a layer of mushroom-like particles (Fig. 2c). XRD patterns show that some weak diffraction peaks of Cu_2S (JCPDS 84-207) appearing when the Cu foil gets through the vulcanization process (Fig. 2d), demonstrating that Cu_2S was successfully grown on the surface of the Cu foil. The thickness of the Cu foil is 14 μm (Fig. 2e), while that of the Cu_2S/Cu foil increases to around 19 μm (Fig. 2f). From the corresponding backscattering electron image of the Cu_2S/Cu foil (Fig. 2g), a layer of Cu_2S is *in situ* grown on the surface particle of the Cu foil. The results of energy disperse spectroscopy patterns (the insets in Fig. 2g) are also consistent with the corresponding XRD analysis.

With the help of double spherical aberration corrected TEM, we can further observe and confirm that the Cu_2S layer *in situ* grown on the Cu foil. Fig. 3a shows the HAADF image of the prepared Cu_2S/Cu foil. Fig. 3b and c show the atomic resolution HAADF images of selected areas. The former image, along the [114] zone axis, matches with CuO (Fig. 3b), which results from the surface oxidation during sample preparation; the latter image, along the [110] and [010] zone axes, corresponds to Cu_2S (Fig. 3c), which is well consistent with the XRD pattern and energy disperse spectroscopy. These atomic-resolution HAADF images also verify that the blue and magenta rectangular regions in Fig. 3a are the Cu substrate and the Cu_2S layer, respectively. Combined with the atomic resolution HAADF images, the elemental mappings of Cu and S for the whole region of Fig. 3a, shown in Fig. 3d and e, further confirm the phase interface between Cu_2S and Cu (see the red dotted line in Fig. 3a).

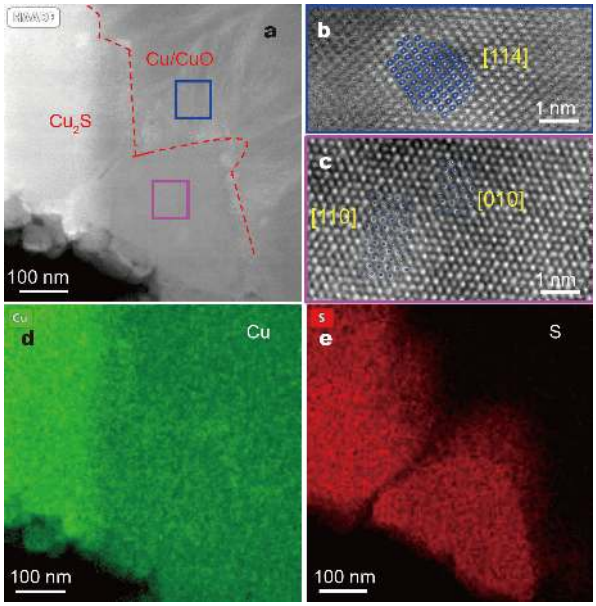

Figure 3 (a) HAADF image of Cu_2S/Cu foil with clear phase interface. Atomic resolution HAADF images of (b) blue and (c) magenta rectangular regions in (a), respectively. Elemental mappings of (d) Cu and (e) S for the whole region in (a).

Fig. 4 displays the morphologies of the Cu foil and Cu_2S/Cu foil after plating different Li contents. When using Cu foil as the current collector, it can be seen that the deposited Li has many cracks and a rough surface at a capacity of 1 mA h cm^{-2} (Fig. 4a). With increasing Li content, there are a lot of dendritic Li, porous and dead lithium, due to non-uniform Li deposition (Fig. 4b–d). For the Cu_2S/Cu foil, the surface morphology is much

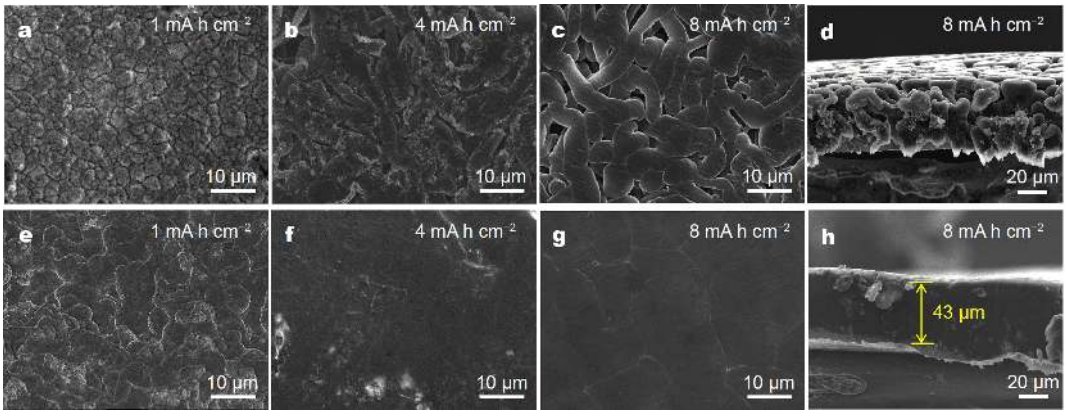

Figure 4 SEM images of the morphologies of Li deposition on (a–d) Cu and (e–h) Cu_2S/Cu current collectors at a current density of 1 mA cm^{-2} with different capacities.

flatter and denser (Fig. 4e–h). When plating a small amount of lithium (1 mA h cm^{-2}), lithium uniformly deposits with no cracking, due to the high lithophilic ability of Cu_2S (Fig. 4e). Even plating a capacity as high as 8 mA h cm^{-2}, the surface is still very smooth and no porous or dendritic Li appears (Fig. 4g). From the cross-sectional image (Fig. 4h), we can see that, after plating at 8 mA h cm^{-2}, the thickness of the deposited lithium on the Cu_2S/Cu foil is about 43 μm, which approaches that on Li foil (40 μm), further indicating that Cu_2S can induce Li depositing and lead to extremely dense deposited lithium with no dead lithium or dendrite. Therefore, the Cu_2S/Cu current collector enables the longer lifespan of a cell, even at a high total capacity.

The SEI layer is a vital factor for Li anode protection. Fig. 5a clearly shows the morphology of the Cu_2S/Cu current collector after five depositing/stripping cycles. It can be seen that there is an intact SEI layer on the surface of the collector. To confirm the composition of the SEI layer, XRD test was carried out for both Cu and Cu_2S/Cu current collectors after five cycles at Li totally stripped status (Fig. 5b). The diffraction peak of Li_2S only appears in the Cu_2S/Cu foil. Combining with XPS spectra of S 2p (Fig. 5c), except for the peaks of Li salt and the oxidized part, it is ensured that Li_2S and Li_2S_2 coexist in the outermost layer of the Cu_2S/Cu foil. To further analyze the SEI layer formed on the surface of Cu_2S, focused ion beam technology was employed to cut the Cu_2S/Cu current collector after five depositing/stripping cycles for cross-sectional HAADF image (Fig. 5d). Fig. 5e shows the EELS of Li in the red rectangular area in Fig. 5d. It can be observed that there is rich Li distribution near the surface of the Cu_2S/Cu foil, while there is almost no Li appearing near the Cu substrate region. This reveals that the SEI only formed on the surface of Cu_2S, so Cu_2S has the benefit of forming a compact SEI layer, which can be also verified in the discharge profile at the first cycle (Fig. 5d). The discharge capacity of Cu foil is nearly zero, due to no reaction occurring between the Cu and Li. By contrast, a clear voltage plateau appeared in the Cu_2S/Cu foil, demonstrating that the surface of Cu_2S can firstly react with the Li before Li plating. This phenomenon may explain why the SEI contain Li_2S and Li_2S_2 [33].

For heterogeneous nucleation of Li, an energy barrier must be overcome, which is usually evaluated by the value of the nucleation overpotential determined by the difference between the voltage dip and the ultimate fat-part of the voltage plateau. Fig. 6a displays the voltage profiles of the Li plating on both Cu and Cu_2S/Cu current collectors at the first cycle. Due to the non-lithophilic ability of Cu (Fig. 2g), the Cu foil exhibits a larger nucleation overpotential of 150 mV. By contrast, the Cu_2S/Cu foil exhibits an extremely low nucleation overpotential of 23 mV, indicating that lithophilic Cu_2S can optimize the Li nucleation behavior and help to induce the uniform deposition of Li. After overcoming the energy barrier for

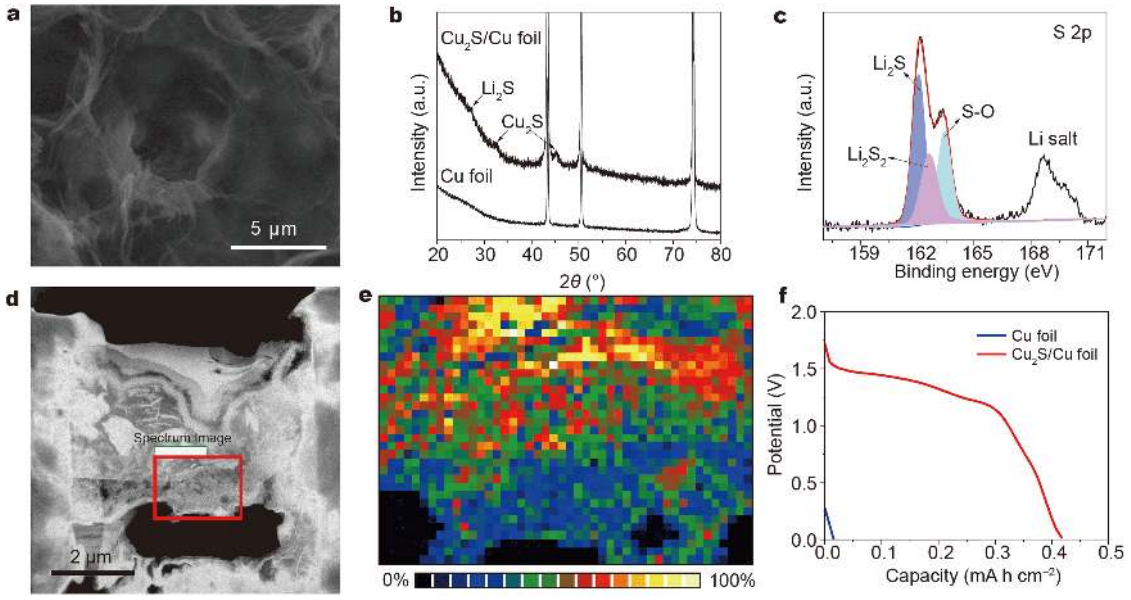

Figure 5 (a) The surface morphology, (c) XPS of S 2p, (d) HAADF image, and (e) EELS of elemental Li in the red rectangular region of (d) for the Cu_2S/Cu current collector after five depositing/stripping cycles; (b) XRD patterns and (f) voltage profiles of both Cu and Cu_2S/Cu foil at the first discharge process.

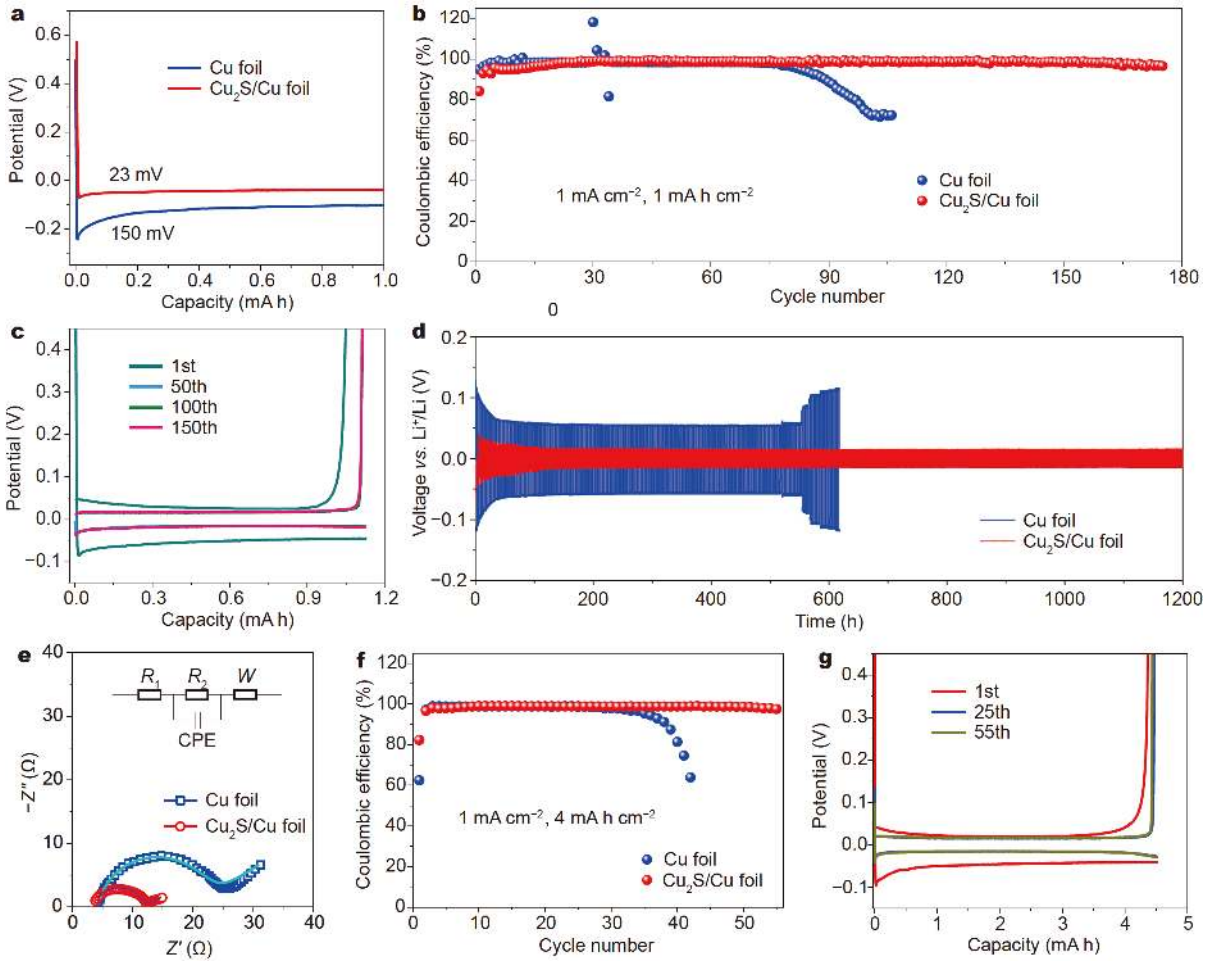

Figure 6 (a) Voltage profiles of Li nucleation on the Cu and Cu_2S/Cu current collectors. Coulombic efficiencies of both Cu and Cu_2S/Cu foils at a current density of 1 mA cm^{-2} with total capacities of (b) 1 mA h cm^{-2} and (f) 4 mA h cm^{-2}. Voltage profiles of Cu_2S/Cu current collectors at a current density of 1 mA cm^{-2} with total capacities of (c) 1 mA h cm^{-2} and (g) 4 mA h cm^{-2}. (d) Voltage-time profiles of symmetric Li||Cu-Li and Li||Cu_2S/Cu-Li cells at 1 mA cm^{-2} with a total capacity of 1 mA h cm^{-2}. (e) EIS of Cu and Cu_2S/Cu foils after 50 cycles.

heterogeneous nucleation of Li, high Coulombic efficiency in every cycle and good cycle stability are essential for the cells. Fig. 6b compares the Coulombic efficiency at a current density of 1 mA cm^{-2} with a total capacity of 1 mA h cm^{-2}. It can be seen that the Coulombic efficiency of commercial Cu foil significantly drops to 70% after only 100 cycles, which can be ascribed to the increased dendritic Li and dead Li induced by the non-uniform lithium deposition during the continuous plating and stripping processes. In contrast, with the protection of the compact SEI layer formed in the initial voltage drop process, the Coulombic efficiency of the Li||Cu_2S/Cu cell maintains much more stable over 180 cycles. Specifically, except for the first cycle, the charge/discharge curves of the Cu_2S/Cu foil show no change, even after 150 Li plating/stripping cycles (Fig. 6c).

Fig. 6d shows the voltage-time profiles of symmetric Li||Cu-Li and Li||Cu_2S/Cu-Li cells at a current density of 1 mA cm^{-2} with a total capacity of 1 mA h cm^{-2}. The polarization of the symmetric Li||Cu-Li cell obviously increases after 500 h, whereas the symmetric Li||Cu_2S/Cu-Li has excellent stability up to 1200 h. In addition, the latter exhibits a much lower overpotential than the former during the prolonged cycling process. EIS profiles of both Cu and Cu_2S/Cu foils after 50 cycles at 1 mA cm^{-2} are shown in Fig. 6e; the insets are their equivalent circuit curves. By simulating the impedance, the internal resistance (R_1) of Cu_2S/Cu foil after 50 cycles is 3.36 Ω, lower than that of Cu foil (4.25 Ω), which is mainly attributed to the more uniform Li position. Meanwhile, the interface resistance (R_2) for Cu_2S/Cu foil is 8.48 Ω, only half of that for Cu foil (17.67 Ω), which results from

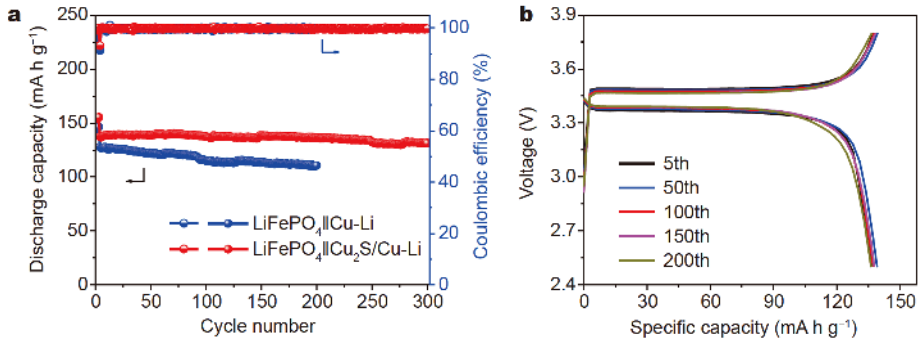

Figure 7 (a) Cycling performance of full-cells consisting of a Cu-Li or Cu_2S/Cu-Li anode and a $LiFePO_4$ cathode at a rate of 1 C. (b) Typical voltage profiles of the full-cell with Cu_2S/Cu anode and $LiFePO_4$ cathode at 1 C.

different amounts of dead Li and side reaction products in the two groups.

High areal capacity loading is crucial to realize high energy density. When increasing the areal capacity to 4 mA h cm^{-2}, the Coulombic efficiency of Cu foil quickly starts to drop after 30 cycles and decreases to about 70% over 40 plating/stripping cycles. With Cu_2S modification, the Coulombic efficiency of the Li metal half cell maintains at about 98%, indicating good reversibility and high utilization of Li during Li plating and stripping. Fig. 6g shows the corresponding voltage profiles of Cu_2S/Cu foil at different cycles, which indicates no change after 55 plating/stripping cycles.

To assess the potential of practical application for Cu_2S/Cu foil in Li metal batteries, two full-cells were assembled with Li-plated Cu foil and Cu_2S/Cu foil (4 mA h cm^{-2}) as the anodes, coupled with a $LiFePO_4$ cathode. The cycling performances of both full-cells were evaluated at a rate of 1 C (Fig. 7a). The $LiFePO_4$||Cu_2S/Cu-Li cell maintains a reversible capacity of 132 mA h g^{-1} with a stable average Coulombic efficiency of 99.6% and a capacity retention of 96% after 300 cycles, much better than that of $LiFePO_4$||Cu-Li, with an average Coulombic efficiency of 99.4% and a capacity retention of 85% after 200 cycles. From the charge-discharge voltage profiles in Fig. 7b, we can see that the $LiFePO_4$||Cu_2S/Cu-Li cell exhibits very stable voltage profiles, even at the 200th cycle, further demonstrating that the Cu_2S layer can effectively ensure the uniform deposition and stripping of Li to avoid dendrite growth.

CONCLUSIONS

We successfully modified commercial Cu foil by a simple one-step vulcanization method to form Cu_2S on the surface of a Cu-based current collector *in situ*. Due to the strong lithophilic ability of Cu_2S, the nucleation overpotential of Li is greatly reduced to 23 mV, and the deposition of Li becomes uniform and compact even with a Li deposition content of up to 8 mA h cm^{-2}. As Cu_2S on Cu foil can help to form an SEI layer containing Li_2S and Li_2S_2 in the initial activation process, the growth of dendritic Li is effectively retarded. Therefore, the Cu_2S/Cu current collector exhibits very stable cycling performance with a high Coulombic efficiency of 97% for more than 180 cycles at a current density of 1 mA cm^{-2} with a total capacity of 1 mA h cm^{-2}. Even when increasing the capacity to 4 mA h cm^{-2}, the Coulombic efficiency can reach 98% for 60 cycles. The symmetric Li||Cu_2S/Cu-Li with low polarization also maintains excellent stability for 1200 h. The full-cell with Cu_2S/Cu foil as the anode and $LiFePO_4$ as the cathode exhibited improved cycling stability and enhanced Coulombic efficiency, demonstrating that the Cu_2S/Cu foil has excellent potential for practical application in Li metal batteries.

Received 10 February 2020; accepted 21 March 2020; published online 29 May 2020

1 Larcher D, Tarascon JM. Towards greener and more sustainable batteries for electrical energy storage. Nat Chem, 2015, 7: 19–29
2 Bruce PG, Scrosati B, Tarascon JM. Nanomaterials for rechargeable lithium batteries. Angew Chem Int Ed, 2008, 47: 2930–2946
3 Zhu Y, Cao T, Li Z, *et al.* Two-dimensional SnO_2/graphene heterostructures for highly reversible electrochemical lithium storage. Sci China Mater, 2018, 61: 1527–1535
4 Li W, Zeng L, Wu Y, *et al.* Nanostructured electrode materials for lithium-ion and sodium-ion batteries *via* electrospinning. Sci China Mater, 2016, 59: 287–321
5 Zhao Y, Ye Y, Wu F, *et al.* Anode interface engineering and architecture design for high-performance lithium-sulfur batteries. Adv Mater, 2019, 31: 1806532
6 Xu W, Wang J, Ding F, *et al.* Lithium metal anodes for rechargeable batteries. Energy Environ Sci, 2014, 7: 513–537
7 Fang C, Wang X, Meng YS. Key issues hindering a practical lithium-metal anode. Trends Chem, 2019, 1: 152–158

8 Chen N, Dai Y, Xing Y, *et al.* Biomimetic ant-nest ionogel electrolyte boosts the performance of dendrite-free lithium batteries. Energy Environ Sci, 2017, 10: 1660–1667
9 Xiang J, Yang L, Yuan L, *et al.* Alkali-metal anodes: From lab to market. Joule, 2019, 3: 2334–2363
10 Wang J, Cui Y, Wang D. Design of hollow nanostructures for energy storage, conversion and production. Adv Mater, 2019, 31: 1801993
11 Cheng XB, Zhang R, Zhao CZ, *et al.* Toward safe lithium metal anode in rechargeable batteries: A review. Chem Rev, 2017, 117: 10403–10473
12 Tobishima S, Takei K, Sakurai Y, *et al.* Lithium ion cell safety. J Power Sources, 2000, 90: 188–195
13 Goriparti S, Miele E, De Angelis F, *et al.* Review on recent progress of nanostructured anode materials for Li-ion batteries. J Power Sources, 2014, 257: 421–443
14 Duan J, Tang X, Dai H, *et al.* Building safe lithium-ion batteries for electric vehicles: A review. Electrochem Energ Rev, 2020, 3: 1–42
15 Lang J, Long Y, Qu J, *et al.* One-pot solution coating of high quality LiF layer to stabilize Li metal anode. Energy Storage Mater, 2019, 16: 85–90
16 Liang X, Wen Z, Liu Y, *et al.* Improved cycling performances of lithium sulfur batteries with $LiNO_3$-modified electrolyte. J Power Sources, 2011, 196: 9839–9843
17 Li W, Yao H, Yan K, *et al.* The synergetic effect of lithium polysulfide and lithium nitrate to prevent lithium dendrite growth. Nat Commun, 2015, 6: 7436
18 Liu QC, Xu JJ, Yuan S, *et al.* Artificial protection film on lithium metal anode toward long-cycle-life lithium-oxygen batteries. Adv Mater, 2015, 27: 5241–5247
19 Liu Y, Lin D, Yuen PY, *et al.* An artificial solid electrolyte interphase with high Li-ion conductivity, mechanical strength, and flexibility for stable lithium metal anodes. Adv Mater, 2017, 29: 1605531
20 Pathak R, Chen K, Gurung A, *et al.* Ultrathin bilayer of graphite/SiO_2 as solid interface for reviving Li metal anode. Adv Energy Mater, 2019, 9: 1901486
21 Luo J, Fang CC, Wu NL. High polarity poly(vinylidene difluoride) thin coating for dendrite-free and high-performance lithium metal anodes. Adv Energy Mater, 2018, 8: 1701482
22 Seino Y, Ota T, Takada K, *et al.* A sulphide lithium super ion conductor is superior to liquid ion conductors for use in rechargeable batteries. Energy Environ Sci, 2014, 7: 627–631
23 Tatsumisago M, Mizuno F, Hayashi A. All-solid-state lithium secondary batteries using sulfide-based glass-ceramic electrolytes. J Power Sources, 2006, 159: 193–199
24 Wu H, Zhang Y, Deng Y, *et al.* A lightweight carbon nanofiber-based 3D structured matrix with high nitrogen-doping level for lithium metal anodes. Sci China Mater, 2018, 62: 87–94
25 Duan H, Zhang J, Chen X, *et al.* Uniform nucleation of lithium in 3D current collectors *via* bromide intermediates for stable cycling lithium metal batteries. J Am Chem Soc, 2018, 140: 18051–18057
26 Lin D, Zhao J, Sun J, *et al.* Three-dimensional stable lithium metal anode with nanoscale lithium islands embedded in ionically conductive solid matrix. Proc Natl Acad Sci USA, 2017, 114: 4613–4618
27 Lyu Z, Lim GJH, Guo R, *et al.* 3D-printed electrodes for lithium metal batteries with high areal capacity and high-rate capability. Energy Storage Mater, 2020, 24: 336–342
28 Cho I, Gong S, Song D, *et al.* Mussel-inspired polydopamine-treated copper foil as a current collector for high-performance silicon anodes. Sci Rep, 2016, 6: 30945
29 Jiang J, Nie P, Ding B, *et al.* Effect of graphene modified Cu current collector on the performance of $Li_4Ti_5O_{12}$ anode for lithium-ion batteries. ACS Appl Mater Interfaces, 2016, 8: 30926–30932
30 Yang CP, Yin YX, Zhang SF, *et al.* Accommodating lithium into 3D current collectors with a submicron skeleton towards long-life lithium metal anodes. Nat Commun, 2015, 6: 8058
31 Zhang SS, Fan X, Wang C. A tin-plated copper substrate for efficient cycling of lithium metal in an anode-free rechargeable lithium battery. Electrochim Acta, 2017, 258: 1201–1207
32 Deng D, Lee JY. Direct fabrication of double-rough chestnut-like multifunctional Sn@C composites on copper foil: Lotus effect and lithium ion storage properties. J Mater Chem, 2010, 20: 8045
33 Huang Z, Zhang C, Lv W, *et al.* Realizing stable lithium deposition by *in situ* grown Cu_2S nanowires inside commercial Cu foam for lithium metal anodes. J Mater Chem A, 2019, 7: 727–732

Acknowledgements This work was supported by the National Key R&D Program of China (2018YFB0905400), the National Natural Science Foundation of China (51632001 and 51972131) and Chinese Postdoctoral Science Foundation. We thank the technical support from the Analytical and Testing Center of Huazhong University of Science and Technology (HUST) for material characterizations. We also thank Tang DG for help with XPS analysis from Key Laboratory of Catalytic Conversion and Energy Material Chemistry of Ministry of Education of South-Central University for Nationalities.

Author contributions Li Z and He D conceived the project. He D designed and engineered the samples. Liao Y, Cheng Z, and Sang X helped with the characterization. He D wrote the paper with support from Li Z and Huang Y. All authors contributed to the general discussion.

Conflict of interest The authors declare no competing interest.

Danqi He is currently a post-doctoral fellow in the Department of Materials Science and Engineering, Huazhong University of Science and Technology (HUST), China. She received her PhD degree from the State Key Laboratory of Advanced Technology for Materials Synthesis and Processing of Wuhan University of Technology (WUT), China. Her research focuses on lithium–metal batteries and lithium-sulfur batteries.

Zhen Li received his PhD degree from HUST in 2014. He worked as a R&D engineer at Amperex Technology Limited (ATL) from 2009 to 2011 and worked as a postdoctoral researcher in Nanyang Technological University (NTU) from 2015 to 2018. In 2018, he became a professor of materials science in HUST. His research interests are lithium-ion batteries, lithium–sulfur batteries, and solid-state batteries.

Yunhui Huang received his BS, MS, and PhD degrees from Peking University. From 2002 to 2004, he worked as an associate professor at Fudan University. He then worked with Prof. John B. Goodenough at the University of Texas at Austin for more than three years. In 2008, he became a chair professor of materials science at HUST. His research group works on rechargeable batteries and electrode materials.

利用简单硫化处理的铜箔获取稳定的金属锂负极

贺丹琪[1], 廖亚祺[1], 程泽晓[1], 桑夏晗[2], 袁利霞[1], 李真[1*], 黄云辉[1*]

摘要 金属锂被认为是下一代高能量密度二次电池的终极形式. 但是, 金属锂的高活性和枝晶生长严重限制了其商业化应用. 只有实现锂离子的均匀沉积才能解决相关问题. 本研究通过对商业化铜箔进行简单的一步法硫化处理, 在其表面原位生成一层具有亲锂性的Cu_2S修饰层. 该Cu_2S层不仅可以利用其亲锂性促进锂离子的均匀沉积, 而且在初始活化过程中有利于形成稳定的固态电解质界面. 在锂沉积/剥离循环过程中, 这种经过修饰的铜箔集流体有效抑制了锂枝晶生长, 即使在4 mA h cm^{-2}的循环条件下, 也能够展现出较高的库仑效率和稳定的循环性能. 将沉积金属锂后的Cu_2S/Cu-Li复合负极与$LiFePO_4$正极组装成全电池, 其循环稳定性和库仑效率均大幅度提高, 表明该修饰后的铜箔在二次金属锂电池领域具有良好的应用前景.

